Atmos. Meas. Tech., 4, 1705–1712, 2011
www.atmos-meas-tech.net/4/1705/2011/
doi:10.5194/amt-4-1705-2011

Atmospheric Measurement Techniques

Opportunistic validation of sulfur dioxide in the Sarychev Peak volcanic eruption cloud

S. A. Carn[1] and T. M. Lopez[2]

[1]Department of Geological and Mining Engineering and Sciences, Michigan Technological University, 1400 Townsend Drive, Houghton, MI 49931, USA
[2]Geophysical Institute, University of Alaska Fairbanks, 903 Koyukuk Drive, Fairbanks, AK 99775, USA

Received: 6 June 2011 – Published in Atmos. Meas. Tech. Discuss.: 17 June 2011
Revised: 24 August 2011 – Accepted: 25 August 2011 – Published: 1 September 2011

Abstract. We report attempted validation of Ozone Monitoring Instrument (OMI) sulfur dioxide (SO_2) retrievals in the stratospheric volcanic cloud from Sarychev Peak (Kurile Islands) in June 2009, through opportunistic deployment of a ground-based ultraviolet (UV) spectrometer (FLYSPEC) as the volcanic cloud drifted over central Alaska. The volcanic cloud altitude (∼12–14 km) was constrained using coincident CALIPSO lidar observations. By invoking some assumptions about the spatial distribution of SO_2, we derive averages of FLYSPEC vertical SO_2 columns for comparison with OMI SO_2 measurements. Despite limited data, we find minimum OMI-FLYSPEC differences within measurement uncertainties, which support the validity of the operational OMI SO_2 algorithm. However, our analysis also highlights the challenges involved in comparing datasets representing markedly different spatial and temporal scales. This effort represents the first attempt to validate SO_2 in a stratospheric volcanic cloud using a mobile ground-based instrument, and demonstrates the need for a network of rapidly deployable instruments for validation of space-based volcanic SO_2 measurements.

1 Introduction

Validation of satellite retrievals of trace gases is a crucial part of any mission, but the approach is highly dependent on the species in question. Some molecules (e.g., NO_2) have well-characterized sources and somewhat predictable distributions, making it easier to plan validation campaigns and extended deployments of ground-based or airborne instrumentation (e.g., Brinksma et al., 2008). However, this is not usually the case for volcanic SO_2, emitted by largely unpredictable volcanic activity, often in remote locations. Validation of satellite SO_2 measurements in such situations is mostly opportunistic (e.g., Carn et al., 2011), and may require rapid mobilization or deployment of ground-based assets (e.g., Spinei et al., 2010). Efforts to validate volcanic SO_2 retrievals have become increasingly important in the light of recent volcanic ash crises (e.g., the 2010 Eyjafjallajökull eruption), during which satellite measurements of SO_2 and ash were used to track the drifting volcanic clouds (e.g., Thomas and Prata, 2011).

We show here that useful SO_2 validation data can be collected by rapid deployment of a simple, mobile ultraviolet (UV) spectrometer system similar to those used widely for volcano monitoring. The opportunity arose when the volcanic cloud produced by the June 2009 explosive eruption of Sarychev Peak (Matua Island, Kuril Is; 48.1° N, 153.2° E) drifted over central Alaska. Satellite measurements of SO_2 by the Ozone Monitoring Instrument (OMI) on NASA's Aura satellite were the object of validation. Our measurements represent the first attempt to validate SO_2 in a drifting, stratospheric volcanic cloud using road-based vehicular traverses beneath the plume.

The 2009 eruption of Sarychev Peak began on 11 June. Haywood et al. (2010) provide an overview of the eruption and present SO_2 data from the Infrared Atmospheric Sounding Interferometer (IASI) on the MetOp-A satellite, along with climate model simulations of volcanic cloud dispersion. IASI measured a total SO_2 burden of 1.2 ± 0.2 Tg in the upper troposphere and lower stratosphere (UTLS) following the

Correspondence to: S. A. Carn
(scarn@mtu.edu)

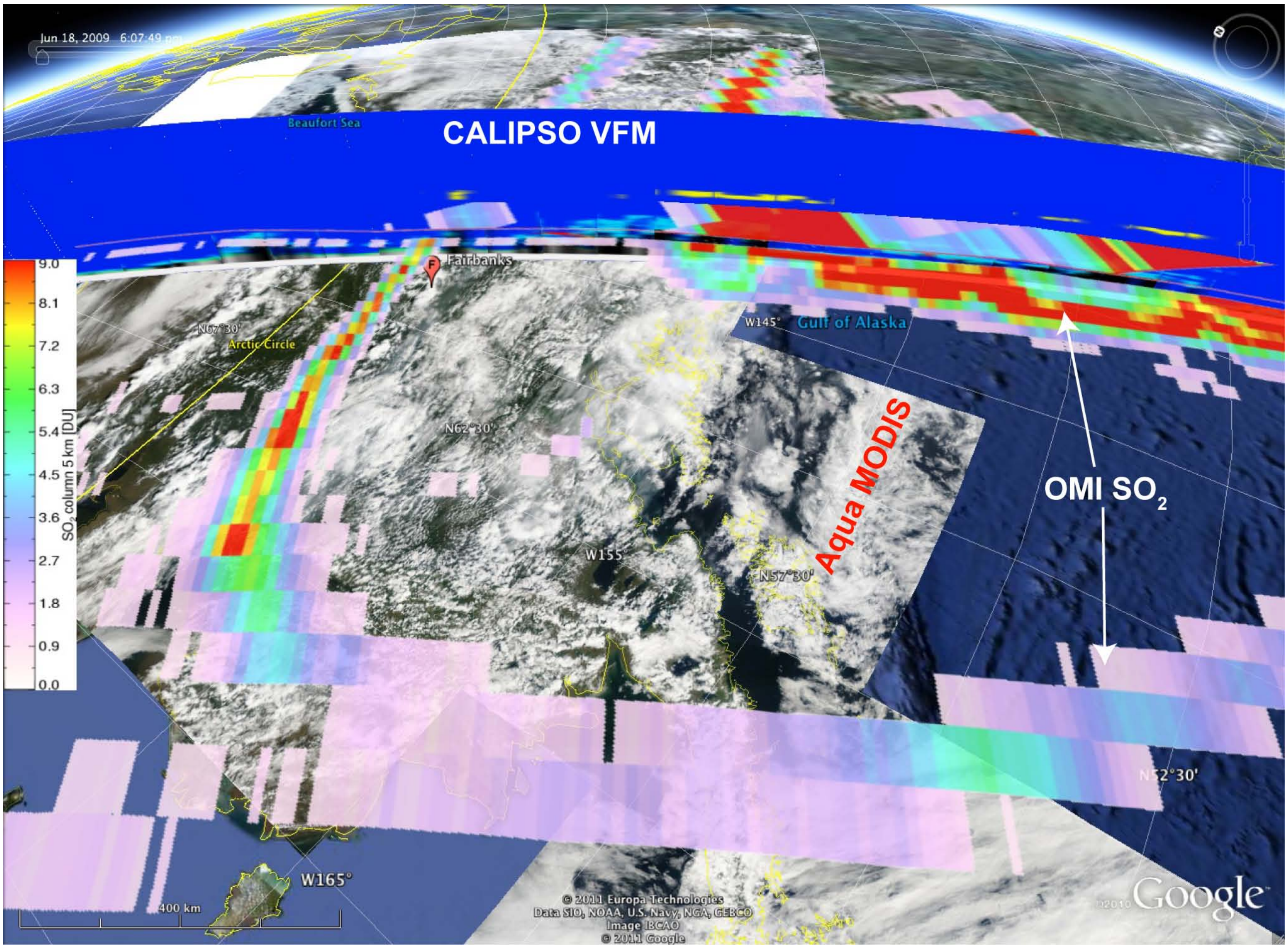

Fig. 1. Google Earth™ composite showing a perspective view of A-Train satellite observations of the Sarychev Peak volcanic cloud over Alaska on 18 June 2009. The datasets shown are true-color Aqua MODIS visible imagery (∼22:20 UTC; *lowermost image*), OMI SO_2 columns (∼22:28 UTC; *large colored pixels* – color scale shown on left) and a CALIPSO lidar Vertical Feature Mask (VFM) curtain (∼22:20 UTC). Yellow features on the CALIPSO VFM curtain indicate stratospheric volcanic aerosol at altitudes of ∼12–15 km. The location of Fairbanks, AK is indicated. The data (KMZ files) used to create this figure are available as a Supplement.

eruption sequence, which is commensurate with total SO_2 burdens measured by OMI. Dispersion of the volcanic SO_2 after eruption was complex but is not the focus of this paper. An animation of OMI SO_2 data showing dispersion of the Sarychev Peak SO_2 cloud over the Northern Hemisphere from 10 June–31 July 2009 is available as Supplementary Online Material. Beginning on 15 June, the SO_2 cloud began to drift across Alaska, providing the opportunity for validation described herein. In contrast to the SO_2 clouds released by the eruptions of Okmok and Kasatochi (Aleutian Islands) in July–August 2008 (e.g., Spinei et al., 2010), the bulk of the Sarychev eruption cloud resided at high latitudes, presenting few opportunities for ground-based measurements.

2 Data

The Level 2 OMI dataset used here is derived from version 003 of the operational SO_2 algorithm (hereafter referred to as OMSO2), the theoretical basis of which is described by Yang et al. (2007). We also use the Level 2 OMPIXCOR OMI Ground Pixel Corner Coordinate product. OMSO2 and OMPIXCOR data are publicly available from the NASA Goddard Earth Sciences (GES) Data and Information Services Center (DISC; http://daac.gsfc.nasa.gov/). Operational OMI SO_2 retrievals require an a-priori assumption of the vertical SO_2 distribution (Yang et al., 2007), which is currently addressed by providing retrieved SO_2 columns corresponding to four different a-priori SO_2 profiles. For this analysis we use the mid-tropospheric (TRM) and lower stratospheric (STL) SO_2 products, which correspond to SO_2 layer center of mass altitudes (CMAs) of ∼7.5

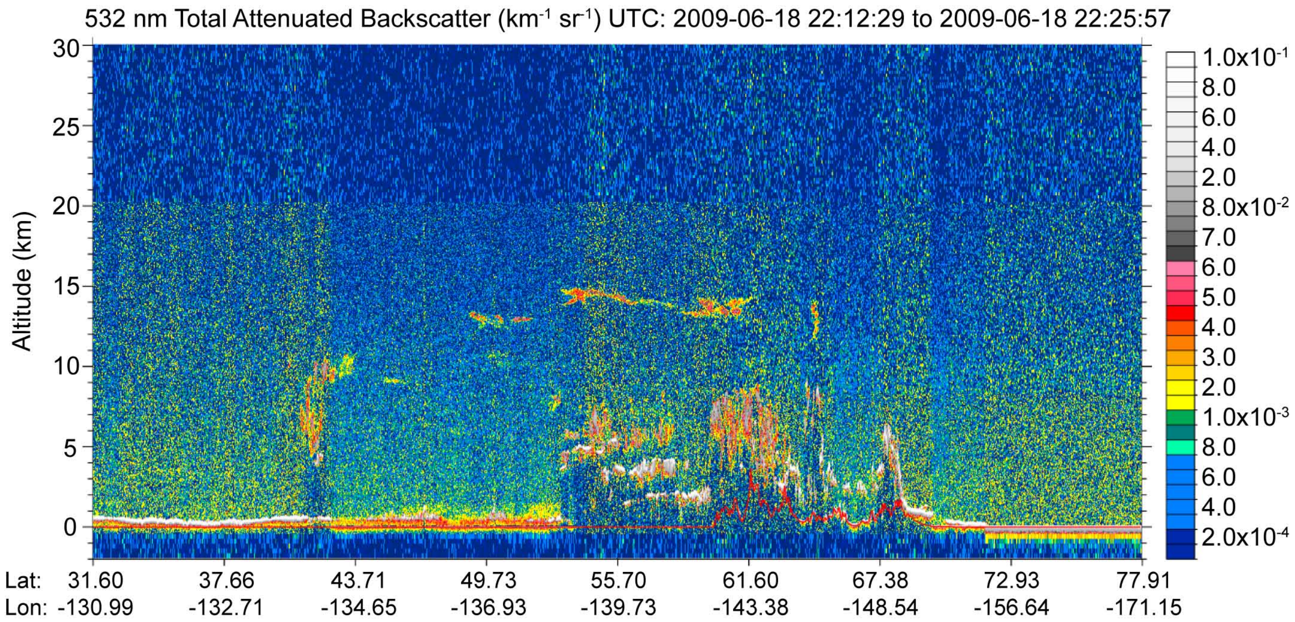

Fig. 2. 532 nm Total Attenuated Backscatter curtain from the Cloud-Aerosol Lidar with Orthogonal Polarization (CALIOP) aboard the CALIPSO satellite, collected at ∼22:12–22:26 UTC on 18 June 2009. This plot and other coincident CALIOP data can be seen at: http://www-calipso.larc.nasa.gov/products/lidar/browse_images/show_date.php?s=production\&v=V3-01\&browse_date=2009-06-18. Features showing elevated backscatter at altitudes above ∼11 km are probably all due to aerosol in the Sarychev Peak volcanic cloud, based on collocation with SO_2 measured by OMI (Fig. 1). Low values of the lidar depolarization ratio in these features (not shown) suggest that the aerosol was dominated by liquid sulfate aerosol and/or liquid-coated solid particles. The volcanic cloud filament discussed in this paper is the northernmost volcanic aerosol feature at ∼64–65° N.

and ∼17.5 km, respectively. Overall uncertainty on the OMI SO_2 retrievals (including CMA errors) for SO_2 clouds above 5 km altitude is ∼20 % (Yang et al., 2007). We also employ other NASA A-Train satellite datasets, including Moderate Resolution Imaging Spectroradiometer (MODIS) data from Aqua, and Cloud-Aerosol Lidar with Orthogonal Polarization (CALIOP) profiles from CALIPSO (Vaughan et al., 2004), to characterize meteorological clouds and assess volcanic cloud altitude (Figs. 1, 2).

Ground-based SO_2 data were collected using a FLYSPEC, a simple but flexible and rapidly deployable UV spectrometer that is calibrated using integral SO_2 gas cells (Horton et al., 2006). Conditions were favorable on 18 June 2009 as the Sarychev SO_2 cloud drifted over southern and central Alaska (Fig. 1; see Supplement). The FLYSPEC was mounted on a vehicle and pointed to zenith, and a high-quality instrument calibration was obtained under clear-sky conditions in Fairbanks (64.84° N, 147.72° W) at 21:06 UTC. Measurements of overhead SO_2 column density were then performed south of Fairbanks along Route 3 towards Healy (Fig. 3), at a roughly constant speed of ∼100 km h^{-1} (∼27 m s^{-1}; Fig. 4). While this speed exceeds that typically recommended for road-based traverses of volcanic SO_2 plumes (10–60 km h^{-1}) (Williams-Jones et al., 2008), it was required by the large extent of the Sarychev SO_2 cloud (Fig. 4). Further FLYSPEC calibrations were performed at 22:27, 22:42, 22:54 UTC on 18 June and 00:22 UTC on 19 June. Conversion of calibrated FLYSPEC data (in ppmm) to column densities in Dobson Units (DU; 1 DU = 0.02848 g m^{-2} SO_2) used the conversion derived by Gerlach (2003) (1 ppmm = 2.663×10^{-6} kg m^{-2}). Further mobile and stationary FLYSPEC measurements were also made in Fairbanks on 20 June, when the Sarychev SO_2 cloud was again overhead. However, in this case the spatially extensive SO_2 cloud precluded FLYSPEC calibration under clear-sky conditions, and these measurements are not discussed further here. Noise in FLYSPEC SO_2 data has been reported to be ∼0.4–1.1 DU, with errors of up to 6 % on retrieved SO_2 columns based on testing with standard calibration cells (Elias et al., 2006).

3 Results and discussion

OMSO2 data show a filament of SO_2 extending across central Alaska in the 22:28 UTC Aura overpass on 18 June 2009 (Fig. 1). CALIOP detected collocated aerosol (presumably sulfate) in the lower stratosphere at ∼12–14 km altitude in the 22:22 UTC CALIPSO overpass (Fig. 2), while Aqua MODIS data indicate partly cloudy conditions and visible haze south of Fairbanks (Fig. 3). Figure 3 shows southbound and northbound FLYSPEC traverses superimposed on the OMI SO_2 retrievals. FLYSPEC traverse profiles, showing

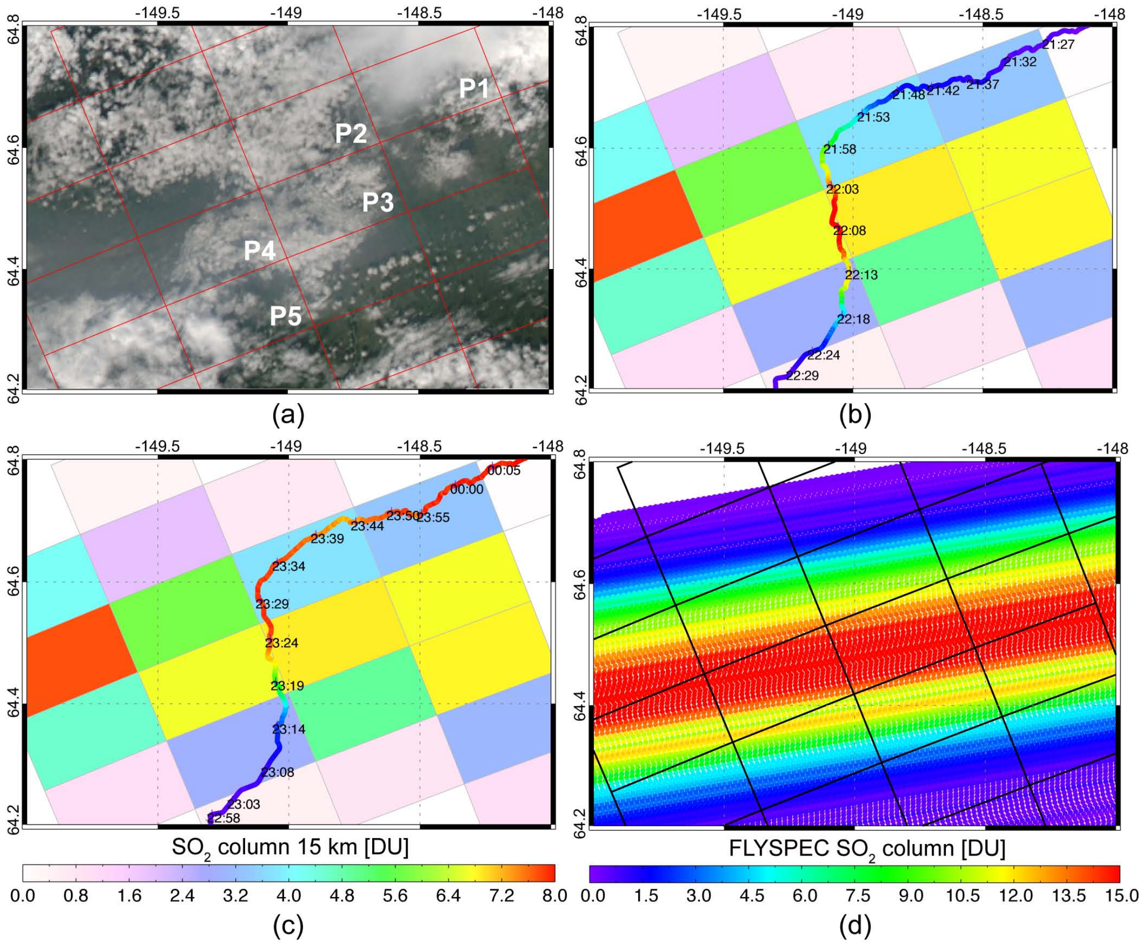

Fig. 3. **(a)** Aqua MODIS visible image of the region south of Fairbanks, AK on 18 June 2009 at 22:20 UTC with OMI pixel boundaries overlain in red (pixel dimensions are $\sim 13 \times 24$ km). OMI pixel numbers correspond to those in Table 1. Note visible haze in the volcanic cloud across image center. **(b)** OMI SO_2 columns (22:28 UTC; *colored pixels*) and ground-based FLYSPEC SO_2 traverse southbound from Fairbanks (periodically time stamped in UTC). OMI SO_2 color bar is shown in **(c)**; FLYSPEC data color bar is shown in **(d)**; **(c)** OMI SO_2 columns (22:28 UTC) and ground-based FLYSPEC SO_2 traverse northbound towards Fairbanks; **(d)** lateral extrapolation of southbound traverse FLYSPEC data to assess effects of spatial averaging. OMI pixel boundaries are overlain in black.

a relatively smooth, symmetrical plume cross-section in the southbound traverse, are shown in Fig. 5. The FLYSPEC traverses intersected five near-nadir OMI pixels in orbit 26207 (Fig. 3), and the average FLYSPEC SO_2 columns for each OMI pixel are reported in Table 1. We compute the OMI SO_2 column for SO_2 at 12–14 km altitude (we use 13 km) by linear interpolation between the OMSO2 TRM and STL columns.

One factor that complicates the analysis is that the volcanic cloud was moving northwards during FLYSPEC data collection. Radiosonde soundings from Fairbanks (http://weather.uwyo.edu/upperair/sounding.html) at 12 Z on 18 June and 00 Z on 19 June indicate southerly to southeasterly winds at $\sim$2.6–5.1 m s^{-1} (9.4–18.5 km h^{-1}) at 13 km altitude, but with significant wind shear at 10–12 km. This is consistent with the observation that SO_2 was not detected over Fairbanks at $\sim$21:10 UTC, but had drifted over Fairbanks by 00:15 UTC on 19 June and the northern flank of the plume was not detected in the northbound traverse (Figs. 3, 5). Radiosonde soundings from Anchorage, AK (61.22° N, 149.90° W) and McGrath, AK (62.96° N, 155.60° W) on 18–19 June show similar wind patterns, although we note that the measurement location is situated in the lee of mountainous topography (the Alaska Range) and locally complex wind patterns could have affected the SO_2 cloud. A consequence of the observed wind speed and direction relative to the size ($\sim 13 \times 24$ km) and orientation of the OMI pixels (Fig. 3) is that significant advection of SO_2 would have occurred on timescales of $\sim$40–80 min (i.e., the time taken for winds at $\sim$10–20 km h^{-1} to travel 13 km). For the spatially heterogeneous Sarychev SO_2 cloud (Fig. 5), this complicates the interpretation of FLYSPEC measurements collected more

Table 1. OMSO2 (orbit 26207; 22:28 UTC) and FLYSPEC data for Sarychev volcanic cloud pixels on 18 June 2009.

Pixel No.	xT[1]	Lat (° N)[2]	Lon (° W)[2]	OMI SO_2 column (DU)			Average FLYSPEC SO_2 column (DU)		Cloud fraction[8]	d $[SO_2]/dt$ ($DU\,h^{-1}$)[9]	Interpolated FLYSPEC SO_2 (DU)[10]
				TRM[3]	STL[4]	Interp.[5]	S. Traverse[6]	N. Traverse[7]			
P1	29	64.70	148.47	3.6	3.4	3.5	1.0 (2.4, 2.1)	14.2 (14.0, 12.3)	0.57	5.7 (5.0, 4.4)	9.2 (9.7, 8.4)
P2	28	64.63	148.93	4.2	3.8	4.0	5.7 (4.5, 3.7)	13.8 (13.9, 10.6)	0.34	4.7 (5.5, 4.0)	11.1 (10.7, 8.3)
P3	28	64.51	148.83	7.8	6.9	7.3	14.5 (14.7, 12.6)	13.9 (12.5, 10.5)	0.25	−0.5 (−1.7, −1.5)	14.0 (13.0, 11.1)
P4	27	64.44	149.29	7.6	6.7	7.1	15.3 (14.5, 12.4)	10.0 (9.8, 8.3)	0.25	−4.5 (−4.2, −3.4)	11.4 (10.9, 9.4)
P5	27	64.32	149.18	3.3	3.0	3.1	6.3 (6.0, 5.0)	2.0 (1.9, 1.6)	0.27	−4.9 (−4.7, −3.9)	2.8 (2.6, 2.2)

[1] OMI cross-track pixel position (1–60; 30 is nadir). [2] Lat, Lon corresponds to center of OMI pixel. [3] Collection 3 OMSO2 data for a SO_2 CMA of 7.5 km (TRM product). [4] Collection 3 OMSO2 data for a SO_2 CMA of 17.5 km (STL product). [5] TRM and STL OMSO2 columns linearly interpolated to a SO_2 cloud altitude of 13 km. [6] Average FLYSPEC SO_2 column for southbound traverse from Fairbanks. Data in parentheses account for unweighted and weighted spatial averaging across the OMI pixel, respectively. [7] Average FLYSPEC SO_2 column for northbound traverse towards Fairbanks. Data in parentheses account for unweighted and weighted spatial averaging across the OMI pixel, respectively. [8] OMI-derived cloud fraction in pixel. [9] Rate of change of SO_2 column in each pixel based on southbound and northbound FLYSPEC surveys. Data in parentheses correspond to unweighted and weighted spatial averages within the OMI pixel, respectively. [10] Estimated average FLYSPEC SO_2 column at time of OMI overpass (22:28 UTC). Data in parentheses correspond to unweighted and weighted spatial averages within the OMI pixel, respectively.

than ∼40–80 min before or after the OMI overpass. This applies to pixel P1 in the southbound FLYSPEC survey, and all pixels with the exception of P5 in the northbound survey (Fig. 5).

Although MODIS data indicate possible meteorological cloud interference, OMI cloud fractions were quite low in most pixels (with the exception of pixel P1; Table 1) and OMI cloud pressures (not shown) imply predominantly low-altitude clouds which would not significantly impact OMI retrievals of stratospheric SO_2. The effect of clouds on the FLYSPEC measurements is unclear, but the general smoothness of the SO_2 cross-sections (Fig. 5a) suggests no significant cloud interference in most pixels.

Comparison between the OMI SO_2 columns and the average FLYSPEC SO_2 columns for each OMI pixel reveals some significant differences (Table 1), but the relative timing of the measurements and spatial averaging of SO_2 over the OMI pixels must be accounted for. In the absence of any ground-based constraints on horizontal variations in SO_2 column, we assessed the effects of spatial averaging using a novel approach facilitated by A-Train satellite synergy. This technique involved extending the FLYSPEC SO_2 columns laterally to simulate the 2-D distribution of SO_2 in the volcanic cloud (Fig. 3d). The azimuth for this extrapolation is constrained using the location of maximum SO_2 in the FLYSPEC profile (64.27° N, 149.03° W; Fig. 5) and the location of the matching volcanic aerosol feature in CALIOP data (64.49° N, 145.96° W; Fig. 2), giving an azimuth of ∼81°. This is qualitatively consistent with the SO_2 distribution mapped by OMI (Fig. 3), but the technique clearly fails to account for any heterogeneity in the volcanic cloud. We then computed the mean of the simulated 2-D SO_2 columns over the OMI pixels (Table 1), resulting in adjustments of only a few percent relative to FLYSPEC traverse averages for some pixels, but more substantial (∼10–130 %; Table 1) for others. Note that for some pixels (e.g., P1 in the southbound survey) the spatial average of the extrapolated FLYSPEC

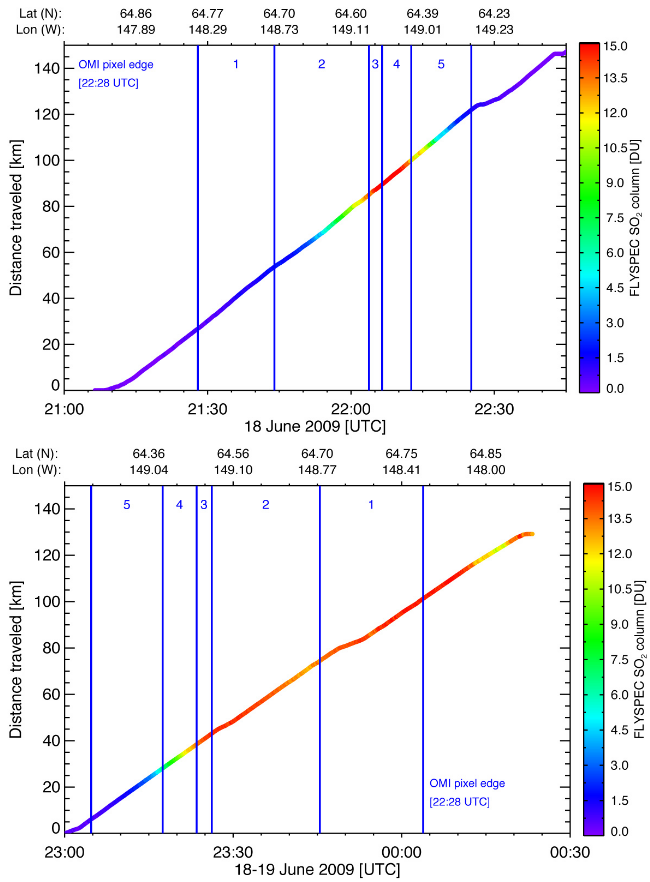

Fig. 4. Distance traveled during (top) southbound and (bottom) northbound FLYSPEC traverses of the volcanic cloud. The distance-time curves are color-coded by SO_2 column amount, and OMI pixel boundaries are indicated. In each case the gradient of the curves yields an approximately constant speed of $\sim 100\,km\,h^{-1}$ ($\sim 30\,m\,s^{-1}$).

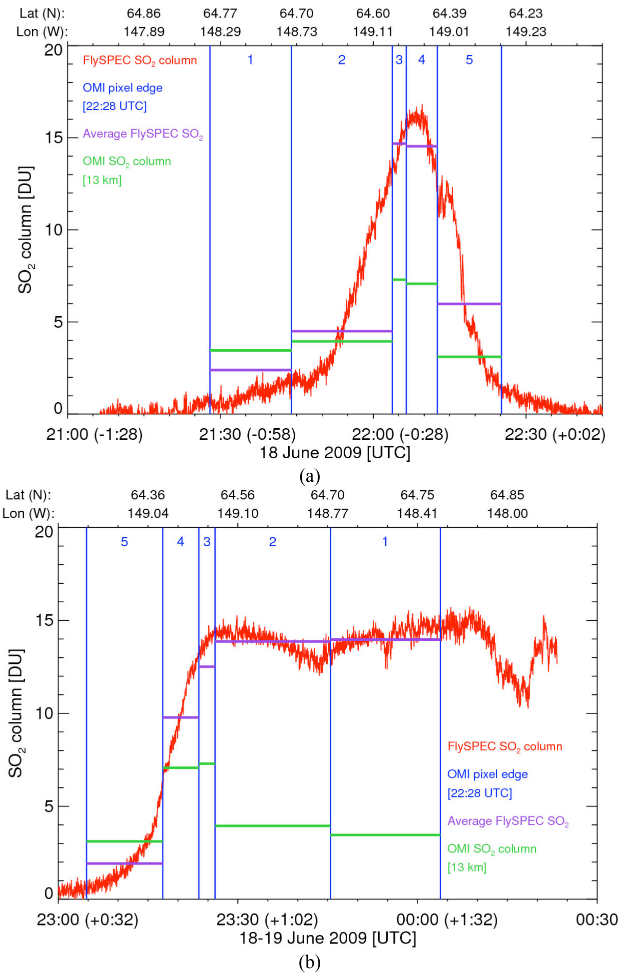

Fig. 5. FLYSPEC SO_2 columns measured during traverses south of Fairbanks (64.84° N, 147.72° W) along Route 3 (red line), OMI pixel boundaries for the 22:28 UTC Aura overpass (vertical blue lines; pixel numbers referred to in Table 1 are shown at top), extrapolated FLYSPEC SO_2 columns averaged (unweighted) over corresponding OMI pixels (horizontal purple lines) and interpolated OMI SO_2 columns in the same pixels (horizontal green lines). The abscissa shows FLYSPEC time; time relative to the Aura overpass is indicated in parentheses. **(a)** Southbound traverse from Fairbanks; **(b)** northbound traverse towards Fairbanks. The absence of a peak in **(b)** is due to northward drift of the volcanic cloud during measurement.

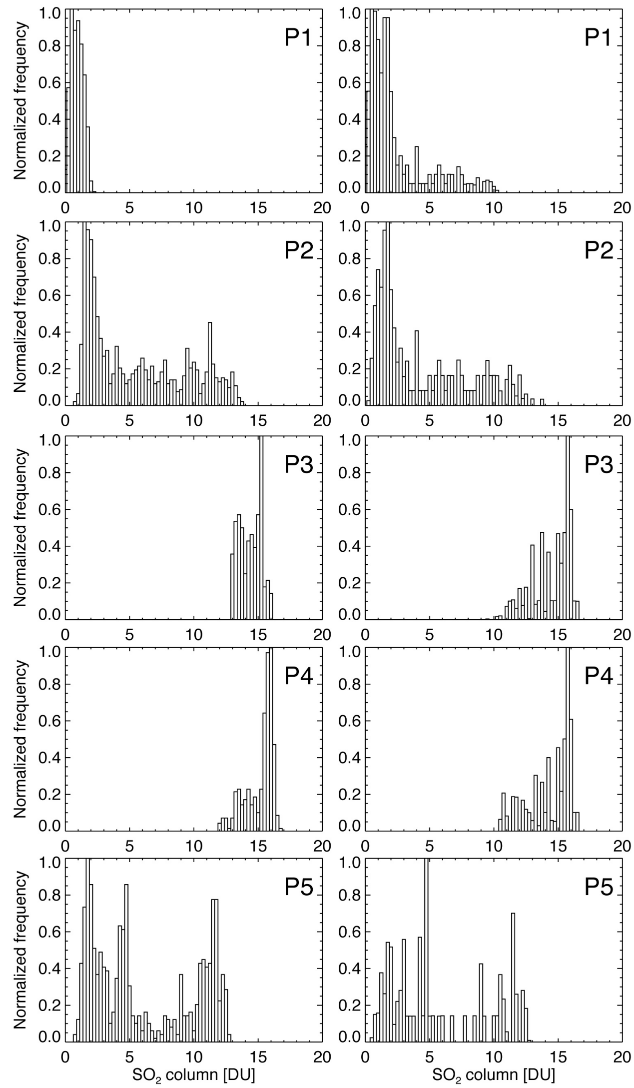

Fig. 6. Histograms of SO_2 column amount for each OMI pixel surveyed by FLYSPEC during the southbound traverse from Fairbanks (Fig. 3). Each histogram pair shows the distribution for raw FLYSPEC measurements on the left, and unweighted spatially-averaged FLYSPEC data on the right. The ordinate shows the number of data points in each bin normalized to the mode.

SO_2 columns exceeds the mean of the raw FLYSPEC data for that pixel (Fig. 5a). In the case of pixel P1, this arises because the FLYSPEC traverse only characterized the northern half of the pixel, whereas the extrapolated SO_2 amounts are higher in the southern half (Fig. 3d).

To account for temporal differences between the OMI and FLYSPEC measurements, we first calculate the temporal gradient in SO_2 column amount for each pixel, based on the FLYSPEC measurements preceding and following the OMI overpass (Table 1). The resulting gradients are $\sim\pm$4–6 DU h^{-1} for all pixels except P3. We then interpolate the SO_2 column amounts for each pixel to the OMI overpass time (22:28 UTC) using these gradients (Table 1). These calculations also allow us to assess the relative magnitude of the spatial and temporal SO_2 gradient for each pixel. In pixels P2, P4 and P5, which were surveyed in ∼20 min or less (Fig. 5), the large spatial gradients in SO_2 column (Figs. 4, 5) in either one or both of the FLYSPEC traverses indicate that adequate spatial characterization was required to validate these pixels. In pixels P1 and P3, the temporal gradient dominates, although as noted above P1 may have been impacted by a large meteorological cloud fraction (Table 1), and P3 is very poorly characterized in the spatial domain (Figs. 3, 4, 5).

Two important results arise from this analysis. Firstly, we find the best agreement between the OMI and spatially averaged FLYSPEC measurements for pixel P2 (13 % difference; Table 1). We attribute this to the fact that pixel P2 has the best FLYSPEC data coverage of all the pixels, both along-track and across-track with respect to the OMI pixel geometry (Fig. 3), providing the best constraints on the sub-pixel SO_2 distribution, despite a ∼30–45 min time difference between the OMI and FLYSPEC measurements. This is corroborated further by inspection of histograms of SO_2 column amount for each pixel (Fig. 6). These histograms show that the FLYSPEC traverse data for pixel P2 best match the mode and distribution of SO_2 column amounts predicted for the entire pixel (Fig. 3d), which is a result of the good spatial characterization of this pixel.

Secondly, we also find good agreement between the OMI measurements (3.1 DU) and the interpolated FLYSPEC data for pixel P5 (∼11–19 % difference; Table 1). We attribute this to the fact that the FLYSPEC data were collected closest in time to the OMI overpass (Fig. 5). For the other pixels, the differences between the FLYSPEC and OMI measurements are significant and generally increase with temporal offset from the OMI overpass time (Table 1). This may indicate that the SO_2 columns in each pixel were changing in a non-linear manner during the period of data acquisition, and hence the assumption of a linear SO_2 column gradient, coupled with uncertainties on the spatial SO_2 distribution, was inadequate for most pixels.

Differences between OMI and spatially averaged FLYSPEC SO_2 columns are larger for the other analyzed pixels, particularly around the location of maximum SO_2 (Table 1; Fig. 5a). This is perhaps best explained by spatial heterogeneity in the volcanic cloud that is not captured in our simple 2-D model of the plume (Fig. 3d). Furthermore, pixels P3 and P4 were not well-characterized by the FLYSPEC data and the traverses were close to the pixel boundaries, where the precise definition of the OMI spatial resolution becomes critical due to the variable OMI pixel spatial response function (SRF). All these factors may have contributed to the lower SO_2 column measured by OMI in these pixels. It is likely that the larger cloud fraction in pixel P1 caused the relatively poor agreement for the southbound traverse (Fig. 3; Table 1). Increasing discrepancies are seen for the northbound FLYSPEC traverse data (Fig. 5b) as by this time the SO_2 cloud had moved north over Fairbanks.

It is important to note here that the spatial resolution of OMI (or any CCD-array based spectrometer) cannot be simply represented by the mapped pixel edges (Figs. 3, 5). The SRF in both the flight- and across-track direction is approximately Gaussian in shape (Dobber et al., 2006). More precisely, the spatial resolution in the flight direction (∼13 km at nadir) is defined as the full-width at half-maximum (FWHM) of the telescope instantaneous field-of-view (IFOV; ∼1°) convolved with a 2-second integration time, while in the across-track direction it is the FWHM of the sum of the Gaussian SRFs of 8 binned OMI CCD pixels (∼24 km at nadir). Therefore, each OMI pixel is also influenced by photons received from beyond the mapped pixel boundaries. A detailed analysis of the OMI spatial resolution is beyond the scope of this paper, but we assessed the effect of non-uniform spatial response by weighting the FLYSPEC SO_2 columns with a flat-topped Gaussian function (of the form $f(x) = \exp(-c(x-x_0)^4)$, where $x-x_0$ is absolute distance from the pixel center (x_0) in the along-track direction, and c is a constant) to simulate an along-track SRF with FWHM corresponding to the mapped pixel boundaries. No attempt was made to account for contributions from beyond the FWHM pixel boundary, or to simulate the across-track SRF. The resulting weighted, spatially averaged FLYSPEC SO_2 columns are ∼13–24 % lower than the unweighted averages (Table 1) and improve some of the comparisons. For pixel P2, the OMI-FLYSPEC difference for the southbound traverse reduces to ∼6 %, but for pixel P5, the OMI-FLYSPEC difference for the interpolated SO_2 column increases to ∼30 %. Significant differences remain for the other pixels, which we conclude is probably due to unconstrained sub-pixel spatial heterogeneity in the volcanic SO_2 cloud.

4 Conclusions

As this study demonstrates, validation of volcanic SO_2 measurements is challenging, since acquisition of high-quality ground-based data may be precluded by time constraints. Nevertheless, we find good agreement between selected OMI and spatially averaged FLYSPEC SO_2 data when some necessary assumptions about the 2-D SO_2 distribution are invoked, providing additional support for the validity of the operational OMSO2 dataset (see also Spinei et al., 2010; Carn et al., 2011). Unresolved spatial heterogeneity in the volcanic cloud on a sub-OMI pixel scale coupled with non-linear temporal changes in SO_2 column amount appear to be the best explanations for other observed OMI-FLYSPEC differences.

On the basis of this analysis, validation of satellite SO_2 measurements in drifting volcanic clouds using sensors mounted on mobile platforms would only be recommended when the SO_2 cloud is moving at a velocity much lower than that of the ground-based (or airborne) sensor. For clouds drifting at higher velocities, stationary ground-based measurements would provide better and more easily interpretable validation data (e.g., Spinei et al., 2010). The advantage of using mobile platforms is that multiple contiguous satellite sensor pixels can be surveyed. Furthermore, our analysis confirms that spatial coverage of pixel areas in both along- and across-track directions should be maximized to increase the likelihood of successful validation.

We conclude by stressing the uniqueness of our FLYSPEC SO_2 dataset for the Sarychev Peak eruption, one of the last decade's largest explosive eruptions. As discussed above, the Sarychev volcanic cloud mostly resided at high

Arctic latitudes, precluding widespread ground-based measurements. Perro et al. (2010) report ground-based Brewer spectrophotometer detection of SO_2 from Sarychev over Eureka, northern Canada on 1 July 2009. To our knowledge, the FLYSPEC SO_2 data presented here are the closest measurements to the eruption in time and location. The successful ground-based measurement of the volcanic SO_2 cloud underlines the need for a widespread network of rapidly deployable instruments in order to successfully validate volcanic SO_2 retrievals from satellite sensors.

Supplementary material related to this article is available online at: http://www.atmos-meas-tech.net/4/1705/2011/ amt-4-1705-2011-supplement.zip.

Acknowledgements. Funding for this work was provided by NASA (award no. NNX09AJ40G for Aura validation). We acknowledge the CALIPSO Science Team, Goddard Earth Science (GES) Data and Information Service Center (DISC), Langley Atmospheric Science Data Center (ASDC) and MODIS Rapid Response system for the provision of CALIPSO and MODIS data products in KMZ format. Two anonymous reviewers provided insightful comments that greatly improved the paper.

Edited by: K. Strong

References

Brinksma, E. J., Pinardi, G., Volten, H., Braak, R., Richter, A., Schönhardt, A., van Roozendael, M., Fayt, C., Hermans, C., Dirksen, R. J., Vlemmix, T., Berkhout, A. J. C., Swart, D. P. J., Oetjen, H., Wittrock, F., Wagner, T., Ibrahim, O. W., de Leeuw, G., Moerman, M., Curier, R. L., Celarier, E. A., Cede, A., Knap, W. H., Veefkind, J. P., Eskes, H. J., Allaart, M., Rothe, R., Piters, A. J. M., and Levelt, P. F.: The 2005 and 2006 DANDELIONS NO_2 and aerosol intercomparison campaigns, J. Geophys. Res., 113, D16S46, doi:10.1029/2007JD008808, 2008.

Carn, S. A., Froyd, K., Anderson, B. E., Wennberg, P., Crounse, J., Spencer, K., Dibb, J., Krotkov, N. A., Browell, E. V., Hair, J. W., Diskin, G., Sachse, G., and Vay, S.: In situ measurements of tropospheric volcanic plumes in Ecuador and Colombia during TC^4, J. Geophys. Res., 116, D00J24, doi:10.1029/2010JD014718, 2011.

Dobber, M. R., Dirksen, R., Levelt, P., van den Oord, G. H. J., Voors, R., Kleipool, Q., Jaross, G., Kowalewski, M., Hilsenrath, E., Leppelmeier, G., de Vries, J., Dierssen, W., and Rozemeijer, N.: Ozone Monitoring Instrument calibration, IEEE T. Geosci. Remote Sens., 44(5), 1209–1238, 2006.

Elias, T., Sutton, A. J., Oppenheimer, C., Horton, K. A., Garbeil, H., Tsanev, V., McGonigle, A. J. S., and Williams-Jones, G.: Comparison of COSPEC and two miniature ultraviolet spectrometer systems for SO_2 measurements using scattered sunlight, B. Volcanol., 68, 313–322, 2006.

Gerlach, T. M.: Elevation effects in volcano applications of the COSPEC, in: Volcanic Degassing, edited by: Oppenheimer, C., Pyle, D. M., and Barclay, J., Geological Society, London, Special Publications, 213, 169–175, 2003.

Haywood J. M., Jones, A., Clarisse, L., Bourassa, A., Barnes, J., Telford, P., Bellouin, N., Boucher, O., Agnew, P., Clerbaux, C., Coheur, P., Degenstein, D., and Braesicke, P.: Observations of the eruption of the Sarychev volcano and simulations using the HadGEM2 climate model, J. Geophys. Res., 115, D21212, doi:10.1029/2010JD014447, 2010.

Horton, K. A., Williams-Jones, G., Garbeil, H., Elias, T., Sutton, A. J., Mouginis-Mark, P., Porter, J. N., and Clegg, S.: Real-time measurement of volcanic SO_2 emissions: validation of a new UV correlation spectrometer (FLYSPEC), B. Volcanol., 68, 323–327, 2006.

Perro, C. W., Duck, T. J., Bitar, L., Nott, G. J., Lesins, G. B., O'Neill, N. T., Eloranta, E., Strong, K., Carn, S. A., Lindenmaier, R., Batchelor, R., Saha, A., Pike-Thackray, C., and Drummond, J. R.: Sarychev volcanic aerosol and chemical measurements over Eureka, Canada, Abstract A51B-0104 presented at 2010 Fall Meeting, AGU, San Francisco, CA, 13–17 December, 2010.

Spinei, E., Carn, S. A., Krotkov, N. A., Mount, G. H., Yang, K., and Krueger, A. J.: Validation of Ozone Monitoring Instrument SO_2 measurements in the Okmok volcanic cloud over Pullman, WA in July 2008, J. Geophys. Res., 115, D00L08, doi:10.1029/2009JD013492, 2010.

Thomas, H. E. and Prata, A. J.: Sulphur dioxide as a volcanic ash proxy during the April-May 2010 eruption of Eyjafjallajökull Volcano, Iceland, Atmos. Chem. Phys., 11, 6871–6880, doi:10.5194/acp-11-6871-2011, 2011.

Vaughan, M., Young, S., Winker, D., Powell, K., Omar, A., Liu, Z., Hu, Y., and Hostetler, C.: Fully automated analysis of space-based lidar data: an overview of the CALIPSO retrieval algorithms and data products, Proc. SPIE, 5575, 16–30, 2004.

Williams-Jones, G., Stix, J., and Nadeau, P. A.: Using the COSPEC in the Field, in: The COSPEC Cookbook: Making SO_2 , edited by: Williams-Jones, G., Stix, J., and Hickson, C., Measurements at Active Volcanoes, IAVCEI, Methods in Volcanology, 1, 63–119, 2008.

Yang, K., Krotkov, N. A., Krueger, A. J., Carn, S. A., Bhartia, P. K., and Levelt, P. F.: Retrieval of large volcanic SO_2 columns from the Aura Ozone Monitoring Instrument: comparison and limitations, J. Geophys. Res., 112, D24S43, doi:10.1029/2007JD008825, 2007.